Engineered symbiont biosensor maps micron-scale sugar gradients in the honeybee gut

Audam Chhun[1,*], Andrew Quinn[1], Théodora Steiner[1], Florian Zoppi[1], Thi Huong Giang Nguyen[1], Philipp Engel[1,*], Yolanda Schaerli[1,*]

[1] Department of Fundamental Microbiology, University of Lausanne, Switzerland

* Corresponding authors: audam.chhun@unil.ch, philipp.engel@unil.ch, yolanda.schaerli@unil.ch

Keywords: biosensor, carbohydrate, gut microbiota, *Snodgrassella alvi*, *Apis mellifera*

Abstract

The honeybee gut microbiota plays a key role in shaping host health and susceptibility to disease. Yet, the nutrient environment it experiences within the gut remains poorly characterized. In particular, little is known about the spatial distribution of nutrients across this community, as resolving such fine gradients *in vivo* has been technically challenging. Here, we engineer the native honeybee symbiont *Snodgrassella alvi* as a living biosensor to quantify the bioavailability of the dietary sugar arabinose within the gut. By expanding the genetic toolkit for *S. alvi* through chromosomal integration of high-burden genes and a suite of low-strength promoters, we achieve stable multi-gene expression without compromising host colonization. The resulting biosensor generates a specific, dose-dependent response to arabinose *in situ*, enabling visualization of sugar gradients across gut-associated bacterial biofilms at micron-scale resolution. Using this system, we show that diet-derived arabinose distribution is highly heterogeneous and can be influenced by the metabolic activity of co-colonizing *Gilliamella* species. These findings highlight how diet composition and microbial specialization generate fine-scale microenvironments within the gut. More broadly, this

work further establishes *S. alvi* as a genetically tractable platform for *in situ* probing of microbial metabolism and nutrient distribution.

Introduction

The honeybee serves as a tractable model to study host-microbe interactions, as their gut harbors a simple, yet specialized bacterial community[1–3]. This microbiota exerts remarkable effects on its host, influencing nutrition[4,5], pathogen resistance[6], immunity[7], detoxification[8], behavior[9,10] and cognitive development[11]. Chemical cues from both host and bacteria structure the community and govern these host-microbe and microbe-microbe interactions[12–14]. More specifically, it is the micron-scale distribution of those metabolites, rather than average levels, that dictates niche occupancy, cross-feeding and host phenotypes[15–17]. However, the gut chemical landscape remains challenging to spatially resolve *in situ*: the gastrointestinal tract is a highly dynamic, poorly accessible system with strong spatial heterogeneity.

Microsensors have profiled steep radial oxygen gradients and longitudinal pH variations at millimeter resolution in the bee gut[14]. In contrast, dietary carbohydrates, abundant from pollen and nectar, remain largely unmapped at comparable spatial scales, despite their central role in host health and disease[18,19], and in the metabolic interplay of gut symbionts[4,20]. Current insight into localized sugar bioavailability is limited to demonstrations of carbohydrate breakdown in the stomach[21], absorption in the midgut[22] and to bulk chromatography- and mass spectrometry-based measurements that average signals across gut compartments[12–14]. Such approaches lose spatial context and ignore the important micro-scale gradients that steer microbial colonization. Tools capable of resolving carbohydrates *in vivo* with high spatial precision are therefore critical to advance our understanding of gut microbiota function within its native context.

Some progress toward spatial gut chemistry has been made in mice[23] and some select invertebrates[24,25] but have not been applied to insect models to the best of our

55 knowledge. For instance, spatial host-microbe sequencing and correlative mass
56 spectrometry imaging with fluorescence *in situ* hybridization have recently allowed
57 unprecedented characterization of the mouse gut microenvironments[23,26,27]. Yet, these
58 approaches often have limited sensitivity and resolution for small sugars, while requiring
59 costly instrumentation and low throughput workflows. Another strategy is to deploy
60 engineered symbionts as live biosensors to provide fine-scale, sensitive mapping of
61 relevant metabolites directly in the gut[28,29]. In honeybees, we previously engineered the
62 core symbiont *Snodgrassella alvi* to respond to the synthetic inducer IPTG, demonstrating
63 the feasibility of cell-based sensing in this system and laying the groundwork for
64 developing biosensors for ecologically relevant carbohydrates in the bee gut
65 environment[30].

66 Previous studies identified *Gilliamella* and *Bifidobacterium* as the principal
67 degraders of complex carbohydrates in the bee gut[5]. *Gilliamella apicola* co-localizes with
68 *S. alvi* in layered biofilms, suggesting metabolic crosstalk between these species[31].
69 Comparative genomic and metabolomic analysis indicate that they possess
70 complementary metabolic abilities, whereby *G. apicola* deconstructs pollen glycans and
71 ferments released sugars to organic acids that *S. alvi* consumes, in turn potentially
72 allowing it to deplete oxygen and establish an anaerobic environment for the broader
73 community[12,13,32]. Within this carbohydrate pool, arabinose is particularly interesting as
74 high levels can be toxic to bees and only a subset of *Gilliamella* strains can catabolize
75 it[5,33]. This sugar is commonly present in the bee diet, occurring in both nectar and
76 pollen[34,35]. As such, arabinose represents a compelling target molecule for probing
77 nutrient availability and interspecies metabolic coupling.

78 Here, we expand genetic engineering capacity in *S. alvi* by introducing synthetic
79 promoters for fine control of complex circuits and a streamlined method for chromosomal
80 integration of high-burden genes, enabling *S. alvi* to function as a living biosensor for the
81 dietary sugar arabinose. The engineered strain shows a robust dose-dependent response

82 *in vitro* and *in vivo*, and resolves micron-scale variation in arabinose within the gut. In co-
83 colonization with *Gilliamella* strains that differ in carbohydrate metabolism, it reports
84 arabinose consumption in a controlled diet. Leveraging its sensitivity, we uncover strong
85 radial heterogeneity in the spatial distribution of arabinose derived from pollen
86 degradation, resulting in nutrient gradients poised to structure the bee gut community.
87 Together, these results establish engineered symbionts as powerful *in situ* reporters of
88 metabolite bioavailability in the honeybee gut.
89

90 ## Results

91 **Engineering the honeybee symbiont *S. alvi* as a biosensor for arabinose.** Genetic
92 analyses previously demonstrated that *S. alvi* lacks genes for import or utilization of
93 carbohydrates as a carbon source[32]. To enable *S. alvi* to act as a biosensor for arabinose,
94 we set out to genetically reprogram it to both import and respond to this sugar *via* the
95 expression of a fluorescent protein (**Fig. 1a**).

96 To confer *S. alvi* arabinose import capability, we engineered cells to express AraE,
97 a membrane protein responsible for arabinose transport in *Escherichia coli*[36]. Membrane
98 proteins are difficult to express heterologously and prone to acquire mutations due to
99 potential toxicity, requiring tight regulation of gene expression to maintain production at
100 low levels[37,38]. In *S. alvi*, the few promoters that were available only result in high gene
101 expression, while functional plasmid replication origins replicate in medium-to-high copy
102 number, which together often cause instability in genetic circuits[30,39]. To address this
103 limitation, we began by characterizing several synthetic promoters that, although
104 previously published[40,41], had not been evaluated in *S. alvi*. We identified the CP6
105 promoter as promising, with respectively 70% and 50% less activity than the CP25 and
106 PA3 promoters typically used for engineering of this species[30,42] (**Supplementary Fig. 1**).
107 We then aimed to integrate the *araE* gene, driven

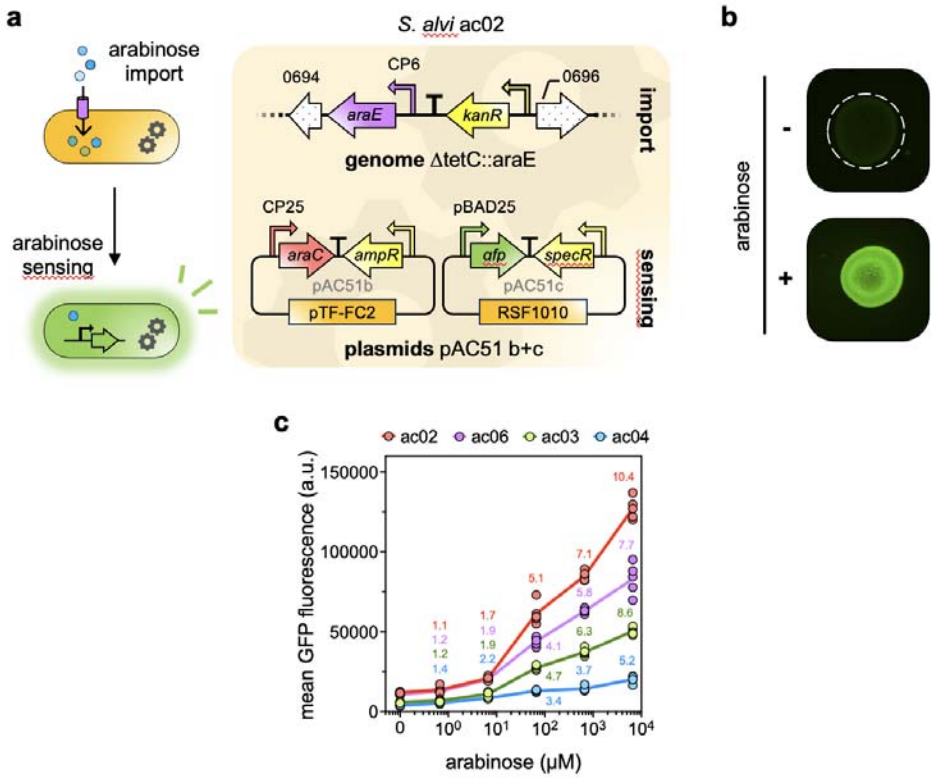

Figure 1. An engineered *S. alvi* strain detects and reports arabinose *in vitro* in a dose-dependent manner. (a) Overview of the genetic engineering carried out in the bee gut symbiont *S. alvi* to acquire arabinose import and sensing capabilities. The *araE* arabinose importer gene was integrated into the genome at the *tetC* locus, enabling arabinose import. Arrows filled with a dotted pattern represent neighboring genes flanking the insertion site and their gene names (SALWKB2_0694 and SALWKB2_0696) are shown above. The dual plasmid system pAC51, based on AraC-mediated regulation of the new synthetic arabinose-inducible promoter pBAD25, enabling arabinose sensing is also depicted. **(b)** Engineered *S. alvi* respond to arabinose by expressing GFP. Top-view images of bacterial lawns inoculated from 10 μl of cells (OD ~ 0.5) and grown on solid media for 3 days, with (+) or without (-) 13 mM arabinose. Dotted-line outlines the shape of a non-fluorescent bacterial lawn. Photos were captured with a Fusion FX device (F-740 filter) using identical exposure times. (c) Variant *S. alvi* strains engineered for arabinose sensing display distinct response profiles. The graph shows mean GFP fluorescence values from 5 biological replicates. Each replicate value was obtained from the average fluorescence of at least 9,000 bacteria measured by flow cytometry. The data lines are color-coded by strain, with the corresponding strain names (ac02-ac06) shown above the plot. Mean fluorescence fold-change relative to the uninduced condition is indicated in the same color. Overview of genetic modifications for each strain can be found in Supplementary Fig. 3C.

109 by the CP6 promoter, into the *S. alvi* genome to minimize its copy number per cell. The
110 previously reported example of targeted genome modification in *S. alvi* used a
111 homologous recombination-based method to insert simple low-burden fluorescent
112 reporters[43]. To achieve stable genomic integration of the membrane-protein encoding
113 *araE* gene, we built upon this approach by developing a suite of standardized primers
114 and plasmids containing different antibiotic resistance cassettes, allowing
115 straightforward and versatile gene integration in *S. alvi* (**Supplementary Fig. 2a**). The
116 constructs, referred to as suicide plasmids, are based on the conditional R6K origin of
117 replication, which functions exclusively in strains expressing the *pir* gene. As a result,
118 antibiotic-resistant *S. alvi* colonies can only arise through integration of the insert
119 fragment, rather than replication of residual plasmids originating from the initial PCR
120 reaction. We used these plasmids to pair the homology arms with an antibiotic cassette
121 (kanR) and combined them in an overlap PCR with *araE* to generate a linear fragment for
122 the *araE* knock-in. This strategy circumvented DNA replication in *E. coli*, thereby avoiding
123 potential *araE*-associated toxicity and minimizing mutation risk (see Materials and
124 Methods and **Supplementary Fig. 2b**). Ultimately, using this optimized genome
125 engineering pipeline, we successfully integrated a genetically stable copy of the *araE*
126 gene into the genome of *S. alvi* (**Fig. 1a**).

127 Next, to enable *S. alvi* to detect and respond to imported arabinose, we
128 engineered a dual plasmid system in which AraC-mediated regulation drives GFP
129 expression in response to the sugar (**Fig. 1a**). In this design, *araC* and *gfp* are encoded on
130 separate plasmids, as we previously found that multi-gene constructs are genetically
131 unstable and prone to mutations in *S. alvi*[30]. As the commonly used pBAD arabinose-
132 inducible promoter is nonfunctional in this species, we designed pBAD25, a synthetic
133 promoter variant functional in *S. alvi*, to control GFP expression (**Fig. 1a**; **Supplementary**
134 **Fig. 3a**). *S. alvi* was able to respond to the presence of arabinose when engineered with
135 both heterologous expression of the chromosomal *araE* gene and the synthetic pBAD25

136 promoter (**Fig. 1b; Supplementary Fig. 3b**). We then asked how key parameters, such as
137 AraC and AraE expression levels, as well as plasmid copy number, could modulate the
138 cells' response to arabinose. For this, we constructed four *S. alvi* strains carrying
139 variations of our genetic circuits and quantified their responses to a range of arabinose
140 concentrations (**Supplementary Fig. 3c**). Each strain displayed a distinct sugar-response
141 profile characterized by differences in dynamic range, sensitivity and basal leakiness
142 (**Fig. 1c**). Among these, the strain *S. alvi* ac02 exhibited the highest dynamic range and
143 sensitivity, with fluorescence increasing up to 10.4-fold upon exposure to 6.7 mM
144 arabinose relative to uninduced conditions, while maintaining low levels of basal
145 leakiness. Briefly, the strain carries a chromosomally integrated copy of the *araE* importer
146 driven by the low-strength promoter CP6, while the dual plasmid system consists of a
147 pTF-FC2-based plasmid bearing *araC* under constitutive expression from CP25 and a
148 second RSF1010-based plasmid expressing GFP under the control of the inducible
149 promoter pBAD25 (**Fig. 1a**). Based on these results, we concluded that *S. alvi* ac02 was a
150 promising candidate to sense and respond in a dose-dependent manner to arabinose and
151 pursued our work with this strain.
152
153 ***In vitro* characterization of the biosensor strain *S. alvi* ac02.** Having engineered *S. alvi*
154 to detect and respond to arabinose, we next sought to characterize *in vitro* the strain's
155 properties relevant to its function as a gut biosensor. We examined (*i*) the specificity of
156 the response to arabinose; (*ii*) the cell sensitivity to ecologically relevant sugar
157 concentrations, and (*iii*) the stability of the genetic modifications in the absence of
158 selection pressure.
159 The engineered strain needed to distinguish arabinose from structurally related
160 sugars. The honeybee diet is indeed remarkably rich in carbohydrates, including the
161 pentose monosaccharides xylose, ribose and arabinose[33]. These sugars are stereoisomers
162 that differ only in the spatial arrangement of a hydroxyl group. To test if our biosensor

163 responds specifically to arabinose, we grew cells in media supplemented with 0.7 mM of
164 either ribose, xylose or arabinose, and measured their fluorescence levels (**Fig. 2a**). The
165 strain responded selectively to arabinose, with a 6.9-fold increase in GFP signal, while
166 exposure to ribose or xylose resulted in fluorescence levels comparable to the uninduced
167 condition. These results indicate that the engineered strain *S. alvi* ac02 provides a
168 specific and reliable readout of arabinose in the presence of structurally related
169 carbohydrates that are found in the bee diet.

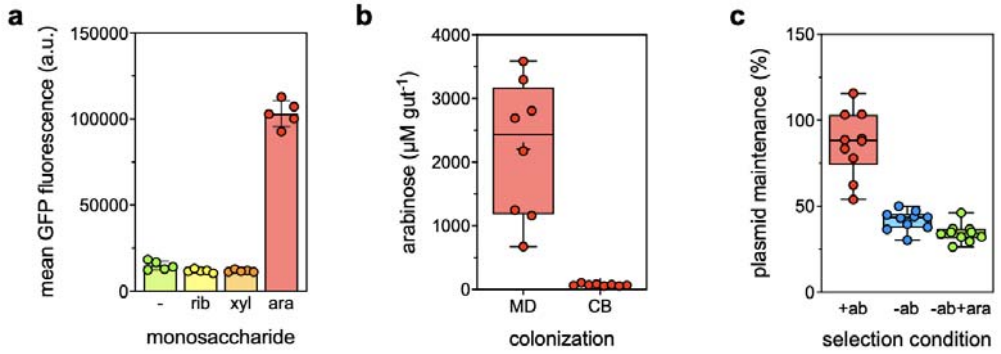

Figure 2. *In vitro* characterization of the biosensor *S. alvi* ac02 properties. (a) *S. alvi* ac02 responds specifically to arabinose. Cells were grown for 3 days in TSB alone (-) or in TSB supplemented with 0.7 mM of ribose (rib), xylose (xyl) or arabinose (ara). Bar plots show mean of GFP fluorescence ± standard deviation of 5 biological replicates. Each replicate value was obtained from the average fluorescence of at least 9,000 bacteria measured by flow cytometry. **(b)** Pollen-derived arabinose concentrations in bee guts. Bees were fed with sugar water and pollen. They were either microbiota-depleted (MD) or colonized (CB) for 7 days prior to dissection and arabinose quantification. Box plots show median arabinose concentrations measured by GC-MS and normalized with the average volume of a bee gut (n = 8). **(c)** Maintenance of arabinose-inducible plasmids pAC51b and pAC51c in *S. alvi* ac02 in the absence of antibiotic selection. Each replicate represents a 3-day liquid culture grown in TSB with ampicillin and spectinomycin (+ab), TSB alone (-ab) or TSB with arabinose (-ab+ara). Plasmid maintenance was calculated as the fraction of CFUs growing on TSA with both antibiotics (*i.e.* cells bearing the two plasmids pAC51b and pAC51c) relative to total CFUs on non-selective TSA. Box plots show median plasmid maintenance of 10 biological replicates.

170

171 We then asked whether the biosensor could respond to sugar concentrations
172 representative of those present in the honeybee gut after pollen digestion. To determine
173 these levels, we dissected guts from pollen-fed, microbiota-deprived (MD) or colonized

174 bees (CB), homogenized them in 500 μL sterile PBS, and analyzed them by mass
175 spectrometry (**Supplementary Fig. 4a**). To convert mass spectrometry values into
176 realistic *in vivo* concentrations, we estimated the average honeybee gut volume, by
177 measuring the mass loss of water after desiccation, to be 19.1 ± 4.7 μl (see Materials and
178 Methods and **Supplementary Fig. 4b**). Using this normalization for the gut volume,
179 arabinose concentrations averaged 2.2 ± 1.1 mM in MD bee guts, and 0.0722 ± 0.0164
180 mM in CB bee guts (n = 8; **Fig. 2b**). This range falls within the detection window of the
181 engineered *S. alvi* strain ac02 (**Fig. 1c**), suggesting it can report variations in arabinose
182 concentrations of both extremes: high concentrations in the absence of microbial
183 metabolism (*i.e.* MD bees) and reduced, ecologically relevant levels when the native gut
184 community consumes arabinose (*i.e.* CB bees).

185 Next, we examined the stability of the genetic circuits in the absence of
186 antibiotics. While part of the biosensor design was chromosomally integrated, we
187 hypothesized that plasmid-borne elements might be lost under non-selective conditions,
188 as expected in the natural gut environment[30]. To test this, we grew *S. alvi* ac02 in liquid
189 tryptic soy broth (TSB) medium with antibiotics (+ab), without antibiotics (-ab), or
190 without antibiotics and arabinose supplementation (-ab+ara; *i.e.* with the circuit
191 activated) and then isolated them onto selective and non-selective solid media. We
192 quantified plasmid maintenance as the fraction of bacteria retaining both plasmids (**Fig.
193 2c**). Under antibiotic pressure, plasmids were stably maintained whereas in its absence
194 maintenance declined to 41.7 ± 5.8 % (-ab) and 34.4 ± 5.3 % (-ab+ara). We found that loss
195 was specific to the *araC*-bearing plasmid pAC51b while the *gfp*-bearing plasmid pAC51c
196 remained stable (**Supplementary Fig. 5a**). Despite this reduction, the absolute number of
197 plasmid-bearing cells remained consequential even when they were exposed to
198 arabinose, with an average of 4.3 10^7 ± 5.3 10^6 CFU ml^{-1} (n = 10; **Supplementary Fig. 5b**),
199 suggesting that enough bacterial biosensors should remain functional in the gut
200 environment.

201

202 **Biosensor-based mapping of arabinose distribution in the honeybee gut.** Building on
203 the *in vitro* demonstration of the biosensor's potential, we next evaluated its performance
204 *in vivo*. Specifically, we focused on whether the engineered strain could establish in the
205 honeybee gut, sense arabinose *in situ* and provide spatial information on sugar
206 availability.

207 First, we assessed the biosensor ability to colonize the honeybee gut. For this,
208 microbiota-deprived bees were either mono-colonized with the engineered strain *S. alvi*
209 ac02 and fed sugar water with (+ab) or without antibiotics (-ab), or co-colonized with the
210 biosensor and a native undefined community derived from gut homogenate that includes
211 wild-type *S. alvi* (-ab+gc; **Fig. 3a**). We monitored colonization dynamics by quantifying
212 bacterial loads in fecal samples over time. Results showed that even in the absence of
213 antibiotic selection, colonization was highly successful: 100% of mono-colonized bees (25
214 of 25 bees) and 95.6% of co-colonized bees (22 of 23 bees) harbored the biosensor after 7
215 days, with mean bacterial loads of $4.3\ 10^5 \pm 5.7\ 10^5$ CFU μl^{-1} and $6.0\ 10^3 \pm 9.2\ 10^3$ CFU μl^{-1},
216 respectively. However, biosensor abundance declined by day 14, most notably in co-
217 colonized bees, whereas mono-colonized individuals remained colonized albeit to lower
218 bacterial loads ($5.6\ 10^2 \pm 2.3\ 10^3$ CFU μl^{-1}, 68.2% of bee colonized).

219 Having confirmed successful colonization of the honeybee gut, we next
220 investigated the biosensor capacity to sense arabinose *in vivo*. To quantify the *in vivo*
221 response of our biosensor, we mono-colonized bees with *S. alvi* ac02 and fed them sugar
222 water containing varying concentrations of arabinose. We dissected guts and imaged
223 them by confocal microscopy. A low basal level of GFP expression in the absence of
224 arabinose enabled straightforward identification of the biosensor bacteria, even without
225 induction. We confirmed that the engineered strain successfully colonized the honeybee
226 gut and formed biofilms that could be readily visualized (**Fig. 3b**). We then quantified

227 fluorescence intensity with a custom FIJI pipeline that automatically defined the biofilm

228 region. The biosensor strain displayed a

229

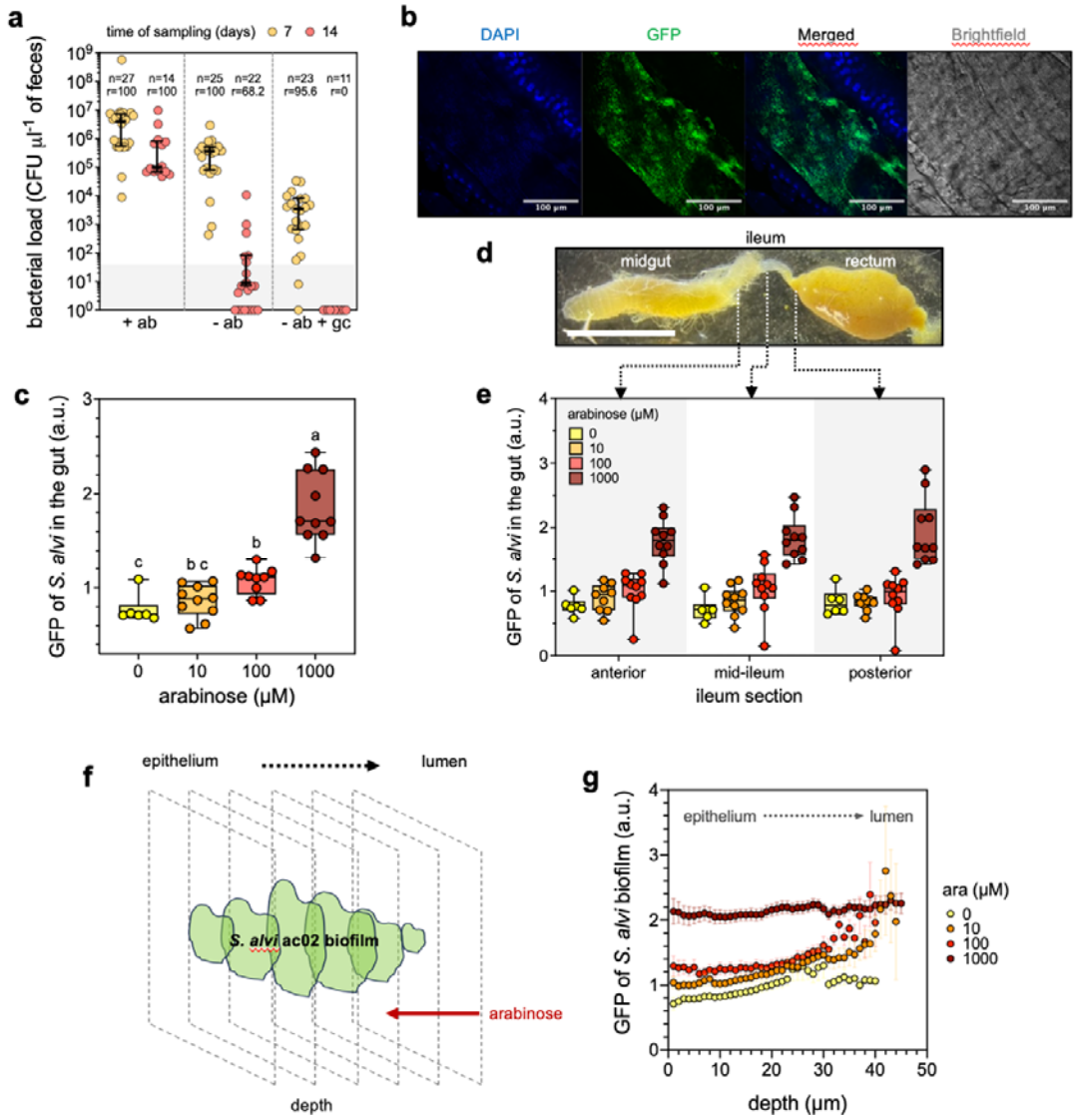

Figure 3. Engineered biosensor enables high-resolution mapping of arabinose in the honeybee gut. (a) Bacterial load of engineered *S. alvi* ac02 cells isolated from bee feces collected 7 (orange) and 14 (red) days after colonization. Bees were either mono-colonized with the biosensor strain and fed sugar water supplemented with (+ab) or without (−ab) antibiotics; or co-colonized with the biosensor strain and the native gut community (-ab+gc). Bees for which engineered bacteria were not detected in the feces were considered non-colonized. The rate of colonized bees (r) and the total number of individuals sampled (n) are indicated. For colonized bees, colored horizontal bars show median values with interquartile ranges. **(b)** A confocal microscopy image of a honeybee gut colonized by engineered *S. alvi* ac02 in the ileum region. A

bacterial biofilm within a gut crypt is shown. The blue channel depicts DAPI staining of host and bacterial DNA and the green channel shows GFP fluorescence from the engineered strain. **(c)** *S. alvi* ac02 responds in a dose dependent manner to arabinose *in vivo*. Box plot shows median value of GFP fluorescence of bacterial biofilms imaged from the gut of bees fed sugar water supplemented with indicated concentrations of arabinose (n = 10). Each fluorescence value corresponds to the average intensity measured from 3 gut sections. Different letters indicate significant differences between arabinose concentrations with adjusted p-value < 0.1 (Tukey HSD test) **(d)** Stereo microscopy image of a honeybee gut. The different gut regions are indicated and separated by white dotted lines. Scale bar represents 5 mm. **(e)** Sugar derived from a simple diet is homogeneously distributed along the longitudinal axis of the honeybee gut. Box plots show median value of GFP fluorescence of *S. alvi* ac02 biofilms found in different gut regions sourced from bees fed sugar water supplemented with varying concentrations of arabinose (n = 10). The regions considered were the anterior (ant) region adjoining the midgut, the mid-ileum (mid) and the posterior (post) region adjoining the rectum. **(f)** Schematic of the microscopy rationale for sugar distribution analysis across bacterial biofilm. **(g)** Sugar derived from a simple diet distributes along a gradient across the depth of *S. alvi* ac02 biofilm. Graph shows mean GFP fluorescence ± SEM of the biosensor according to the biofilm depth. For each bee (n = 10), GFP signal was first averaged over the three ileum regions. The graph displays the average of these per-bee means. Only fluorescence values for which at least two replicates could be measured for a given depth are reported.

clear dose-dependent response to arabinose, with fluorescence increasing significantly with higher arabinose concentrations (**Fig. 3c**).

With colonization and dose-dependent sensing demonstrated, we next examined whether the biosensor could resolve spatial variations in sugar availability both longitudinally (*i.e.* along the length of the gut) and transversally (*i.e.* across the gut). To assess longitudinal variation, fluorescence was measured in three distinct regions of the ileum: the anterior region adjoining the midgut, the mid-ileum and the posterior region adjoining the rectum (**Fig. 3d**). The biosensor reported fluorescence intensities consistent with the arabinose concentrations fed to the host but exhibited no longitudinal variation, with similar fluorescence levels across all three regions for a given sugar condition (**Fig. 3e**). These results indicate that arabinose is homogeneously distributed along the ileum's length.

243 Having established longitudinal uniformity, we next asked whether arabinose
244 availability varied transversally (*i.e.* across the bacterial biofilm on the host epithelium).
245 We hypothesized that micro-scale nutrient gradients exist in these biofilms, because cells
246 located closer to the lumen typically experience higher nutrient access, while those
247 deeper in the biofilm encounter reduced concentration[44,45]. To test whether our biosensor
248 could resolve such fine-scale gradients, we performed confocal imaging with 1 μm depth
249 increments, tracking biofilms of the engineered cells from their epithelial attachment sites
250 to the gut lumen (**Fig. 3f, Supplementary Fig. 6**). In bees fed no arabinose, fluorescence
251 remained uniform across the biofilm depth, whereas a progressive increase in
252 fluorescence toward the lumen was observed in bees fed 10 and 100 μM arabinose,
253 revealing a sugar gradient within the biofilm (**Fig. 3g**). Notably, in bees fed 1,000 μM
254 arabinose, the fluorescence signal was evenly distributed throughout the biofilm,
255 consistent with sugar saturation within the biofilm matrix. Together, these results
256 validate the *S. alvi* biosensor as a *in vivo* reporter capable of resolving transversal sugar
257 gradients within gut biofilms, while revealing longitudinal uniformity along the ileum.
258
259 ***In vivo* mapping of pollen-derived arabinose gradients in bees colonized with**
260 ***Gilliamella*.** After establishing that engineered *S. alvi* resolves *in vivo* arabinose gradients
261 under a simplified diet, we used it to probe the spatial distribution of pollen-derived
262 sugar during co-colonization with members of the genus *Gilliamella*.
263 Genomic analysis suggests divergent arabinose metabolism between the strains
264 *G. apis* ESL169 and *G. apicola* ESL309. The former lacks genes involved in arabinose
265 import and catabolism, whereas the latter has the gene to use this sugar as a carbon
266 source. To visualize strains *in situ*, both *Gilliamella* strains were tagged with a plasmid
267 encoding for the fluorescent reporter E2-crimson, allowing to discriminate the cells from
268 GFP-expressing *S. alvi*. We co-colonized honeybees with the *S. alvi* biosensor and either
269 *G. apis* ESL169 or *G. apicola* ESL309 (**Fig. 4a**), housed the bees in cup-cages and fed them

one of three diets: (*i*) simple sucrose sugar water (SW), (*ii*) SW supplemented with arabinose or (*iii*) SW and pollen *ad libitum*. After 7 days, we dissected the guts and imaged them by confocal microscopy. Image analysis confirmed that both the *S. alvi* engineered strain and *Gilliamella* could successfully colonize the honeybee gut and co-localized in the ileum as layered biofilms (**Fig. 4b**).

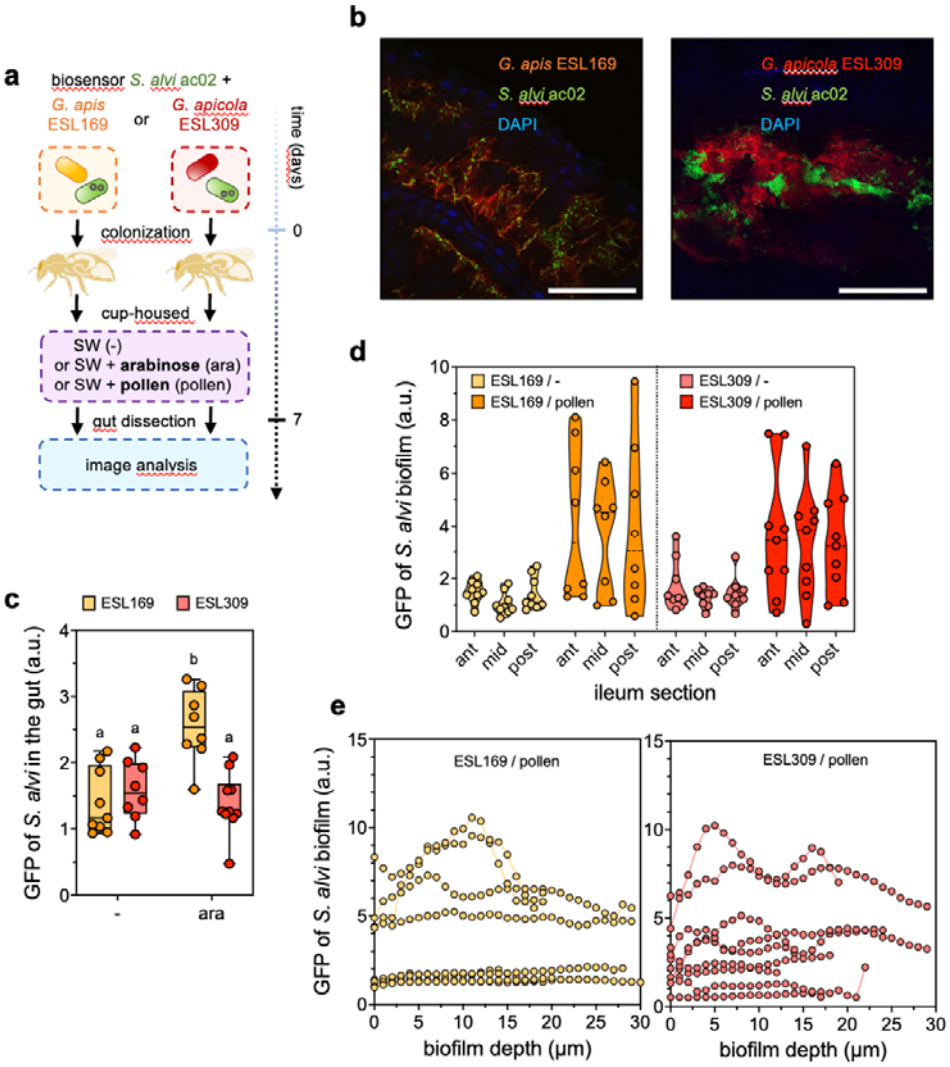

Figure 4. Biosensor mapping reveals heterogenous arabinose gradients from pollen degradation. (a) Schematic outline of the *in vivo* experiment workflow. **(b)** Confocal microscopy images of a honeybee ileum co-colonized by *S. alvi* ac02 and *G. apis* ESL169 (left) or *G. apicola* ESL309 (right). The blue channel depicts DAPI staining of host and bacterial DNA. The green channel shows GFP fluorescence from the engineered *S. alvi* strain. Red channel shows E2-crimson fluorescence from the *Gilliamella* strains transformed with the pAC09 plasmid. Scale bar represents 100 μm. **(c)** *G. apicola* ESL309 catabolizes arabinose whereas *G. apis* ESL169

does not. Box plot shows median value of GFP fluorescence of *S. alvi* biofilms imaged from the gut of bees fed sugar water (-) or sugar water supplemented with 210 μM arabinose (ara). Each fluorescence value corresponds to the overall mean intensity averaged from 3 sections (anterior, mid-ileum, posterior) of one gut and across the depth of the bacterial biofilm for each section. Different letters indicate significant differences in fluorescence intensities across colonization and diet conditions, with adjusted p-value < 0.05 (Tukey HSD test). **(d)** Distribution of pollen-derived arabinose is longitudinally uniform along the ileum. Truncated violin plot shows median value of GFP fluorescence quantified from *S. alvi* biofilms imaged in the gut of bees fed sugar water (-) or sugar water and pollen *ad libitum* (pollen). Each fluorescence value corresponds to the mean intensity averaged across the depth of the bacterial biofilm for each gut section. **(e)** Arabinose derived from pollen breakdown distributes with high heterogeneity along a radial gradient across the depth of *S. alvi* ac02 biofilm when co-colonized with *G. apis* ESL169 (left) or *G. apicola* ESL309 (right). Graphs show the mean GFP fluorescence of the biosensor according to the biofilm depth of individual bees. Data corresponding to the anterior ileum region are displayed only for clarity. Complete data are provided in Supplementary Fig. 8.

We next aimed to confirm the metabolic abilities of the *Gilliamella* strains with regards to arabinose *in vivo*. For this, we quantified *S. alvi* fluorescence across colonization states and diets. The biosensor was induced only in arabinose-fed bees co-colonized with *G. apis* ESL169 (**Fig. 4c**), consistent with arabinose accumulation in the gut. In contrast, no induction was observed with *G. apicola* ESL309, indicating depletion of arabinose by the strain. These results show that the biosensor can report on *in vivo* arabinose consumption and thus validate the divergent sugar metabolisms of the two *Gilliamella* strains tested. Additionally, our observations provide evidence that species-level differences in *Gilliamella* can influence sugar availability in the gut. Having demonstrated the efficacy of the biosensor in this regard, we then leveraged it to map locally the spatial distribution of pollen-derived arabinose.

The pollen-based diet resulted in significant induction of the biosensor, indicating the accumulation of detectable levels of arabinose in the ileum, which were notably independent of the *Gilliamella* species present (**Fig. 4d**). Also, fluorescence measurements of *S. alvi* along the ileum's length revealed highly heterogenous arabinose concentrations between bees, although homogeneously distributed longitudinally and

292 overall consistent within each individual (**Fig. 4d; Supplementary Fig. 7**). By contrast,
293 depth-resolved quantification across *S. alvi* biofilms showed pronounced radial
294 heterogeneity, with arabinose availability varying sharply over microns within a same
295 biofilm and across individuals (**Fig. 4e; Supplementary Fig. 8**). Thus, while arabinose is
296 longitudinally uniform along the ileum, pollen degradation generates patchy, micron-scale
297 nutrients niches within biofilms that differ between bees. These results establish
298 engineered symbionts as sensitive, spatially precise reporters of sugar bioavailability *in*
299 *vivo*, enabling mapping of complex gut chemical microenvironments.
300

301 **Discussion**

302 Here, we engineered the native honeybee gut symbiont *S. alvi* as a living
303 biosensor that reports the bioavailability of the dietary sugar arabinose within the gut. By
304 expanding the genetic toolkit for *S. alvi*, we reprogrammed the bacterium to produce a
305 specific, dose-dependent response to arabinose both *in vitro* and *in vivo*, resolving
306 micron-scale nutrient variation across the gut environment. Using this system, we reveal
307 pronounced spatial heterogeneity in arabinose distribution derived from pollen
308 degradation, uncovering nutrient gradients that likely influence the spatial organization
309 and dynamics of the bee gut microbiota. When co-colonized with distinct *Gilliamella*
310 species, the biosensor reported species-specific arabinose depletion under defined
311 dietary conditions, exposing differences in their carbohydrate metabolism.

312 Our work confirms *S. alvi* as a genetically accessible model system for functional
313 engineering of the bee gut microbiota. Although this species has been engineered before,
314 existing genetic tools could not accommodate complex circuit designs, as only a few
315 high-expression promoters were available[39]. The limited diversity of promoters forced the
316 use of repeated identical sequences across multi-gene constructs and their strong activity
317 imposed substantial metabolic burden, both factors leading to recombinations and
318 mutations[30]. By combining chromosomal integration with a suite of low-strength

319 promoters enabling fine control of gene expression, we overcome these limitations,
320 achieving stable and predictable multi-gene expression in *S. alvi* without compromising
321 its capacity to colonize the gut. This expanded genetic control enhances the tractability of
322 *S. alvi* and broadens its potential as a chassis for *in vivo* studies and microbiome
323 engineering. Extending beyond our previous work with synthetic inducers, it now allows
324 the implementation of more complex functionalities for nutrient biosensing within the gut
325 environment.

326 The ability of an engineered honeybee symbiont to sense and report sugar *in situ*
327 provides a compelling demonstration of how synthetic approaches can provide new
328 insights into previously inaccessible features of gut chemical landscapes. Past efforts to
329 characterize nutrient distribution in animal microbiomes have largely relied on bulk
330 chemical measurements (*i.e.* feces or homogenized gut tissues) or indirect inference using
331 techniques like metagenomics[46] or isotope tracing[47]. These methods fail to capture fine-
332 scale spatial and temporal heterogeneity. In contrast, our biosensor strain enables
333 metabolite detection within the native gut environment, preserving both host and
334 microbial context. Recent advances in spatial metabolomics, especially mass
335 spectrometry imaging, have also begun to probe metabolite distribution *in situ*, typically
336 achieving resolutions in the 3-10 μm range with commercial setups[17,24]. Notably, we could
337 here resolve sugar variation within bacterial biofilms at the 1 μm scale. By engineering
338 biosensing capabilities into a native symbiont with this spatial precision, our approach
339 achieves finely resolved nutrient detection that remains ecologically relevant within its
340 natural niche.

341 This resolution proved particularly powerful under a simplified diet of arabinose-
342 supplemented sugar water, where it revealed a transversal arabinose gradient across
343 bacterial biofilms, with sugar being more accessible closer to the gut lumen. It also
344 enabled the discrimination of species-specific arabinose metabolism among co-colonizing
345 *Gilliamella* species. However, these metabolic differences were no longer detectable

346 under a more complex, pollen-based diet. Instead, the biosensor exposed pronounced
347 radial heterogeneity in arabinose distribution, likely arising from the continued
348 degradation of partially digested pollen grains that can be observed embedded within
349 bacterial biofilms. These residual pollen fragments may act as localized nutrient-release
350 sites, generating patchy, micron-scale variations in sugar availability. The strong
351 heterogeneity in pollen-derived arabinose concentrations observed between bees might
352 also reflect temporal and behavioral effects. For instance, differences in how recently
353 individual bees consumed pollen prior to gut dissection or in how strongly they favored
354 sugar water *versus* pollen feeding. Regardless of its exact origin, this heterogeneity was
355 independent of the *Gilliamella* species present. This is likely due to the high overall
356 arabinose content of pollen, where small-scale depletion by individual species was
357 insufficient to alter the biosensor's response. Alternatively, the presence of pollen-derived
358 metabolites or the limited competition for substrates inherent to this two-member co-
359 colonization may modulate *Gilliamella* metabolism towards reduced arabinose utilization.
360 Nonetheless, these observations demonstrate how diet complexity and pollen breakdown
361 can generate heterogeneous nutrient micro niches within the gut, which can shape
362 microbial interactions at fine spatial scales.

363 Our work establishes a framework for probing the spatial distribution of nutrients
364 in the honeybee gut at an unprecedented resolution, using arabinose as a model
365 substrate. However, pollen degradation releases a much broader spectrum of molecules
366 that includes other carbohydrates, proteins, lipids, amino acids and vitamins[35]. They likely
367 form overlapping chemical gradients shaping community structures and interactions.
368 Indeed, distinct members of the honeybee gut microbiota occupy different metabolic and
369 spatial niches. *Lactobacillus* species, for instance, can utilize sugar alcohols and
370 flavonoids, whereas *Bifidobacteria* dedicate a large fraction of their catabolism to the
371 breakdown of hemicellulose and other complex polysaccharides[5,12,20]. Extending
372 biosensing to these compounds, or simply to other sugars, would provide a more

373 comprehensive view of how diet composition and colonization state structures the gut's
374 metabolic environment. While arabinose has been reported to exert toxicity to honeybees
375 at concentrations more than two orders of magnitude higher than those measured in our
376 study[48], other sugars like mannose are known to adversely affect bees due to inefficient
377 metabolism and accumulation of mannose-6-phosphate[49]. Mapping the distribution and
378 bioavailability of such sugars *in situ* could therefore yield valuable insights into how
379 specific dietary components impact gut function and host physiology. In addition, the
380 sugar composition of bee pollen varies greatly depending on plant origin[50], suggesting
381 that the nutrient landscape experienced by bees feeding on distinct wildflower mixes or
382 single-crop diets may differ substantially. Leveraging our biosensor to monitor how these
383 dietary differences shape metabolite availability would help clarify how food sources
384 could influence the gut environment. Overall, achieving this will require further expansion
385 of the *S. alvi* genetic toolkit, with sensors responsive to a broader range of metabolites
386 and genetic modules supporting more complex circuit designs. In parallel, implementing
387 these biosensors in multi-species or fully reconstituted communities will be essential to
388 capture the metabolic interplay that occurs under natural colonization conditions.
389 Together, these advances would enable high-resolution, community-level mapping of
390 nutrient fluxes and functional specialization within the honeybee gut ecosystem.

391 Finally, our findings highlight the potential of synthetic biology to bridge microbial
392 ecology and functional genomics in natural host systems. By combining genetic
393 engineering with *in situ* readouts, this work demonstrates how non-model symbionts can
394 be transformed into quantitative tools to study metabolism for microbiome research.
395 Expanding such approaches across hosts and microbial taxa will open new avenues to
396 uncover the complex chemical dialogues that underpin host-microbe symbiosis.

397

398 **Methods**

399 **Bacterial strains and culture conditions.** The honeybee gut symbionts *Snodgrassella alvi*
400 wkB2^T (ATTC No. BAA-2449), the engineered biosensor strain *S. alvi* ac02, *Gilliamella*
401 *apicola* ESL309 and *Gilliamella apis* ESL169 were routinely cultured in Tryptic Soy Broth
402 (TSB, Bacto BD). Bacteria were grown at 34 °C under microaerophilic conditions within a 5
403 % CO_2 incubator, with orbital shaking (170 rpm) when required. *Escherichia coli* NEB 5-α
404 (New England Biolabs) and *E. coli* pir+ were employed for plasmid assembly and
405 propagation. *E. coli* strains were grown aerobically in Lysogeny Broth (LB) at 37 °C with
406 orbital shaking (220 rpm). Plasmids were introduced into *S. alvi* by electroporation, and
407 into *Gilliamella* by conjugation, following previously described procedures[30]. When
408 appropriate, antibiotics were added to culture media for selection and plasmid
409 maintenance at the following concentrations: spectinomycin, 30 - 60 μg ml^{-1}; ampicillin, 30
410 - 100 μg ml^{-1}; and kanamycin, 25 - 50 μg ml^{-1}, depending on whether the construct was
411 maintained in *S. alvi*/*Gilliamella* or *E. coli*.
412
413 **Plasmid cloning.** To expand the genetic toolbox for *S. alvi* and enable fine-tuned gene
414 expression, we constructed a panel of plasmids carrying synthetic promoters of varying
415 strengths sourced from a previously published study[40]. Promoters CP25, CP6, CP7, CP32,
416 CP20, J23100, J23106, and J23116 were cloned into the pBTK570 backbone to generate
417 plasmids pAC95, pAC82, pAC83, pAC84, pAC85, pAC86, pAC87 and pAC88, respectively.
418 In each case, the original PA3 promoter driving *E2-crimson* in pBTK570 was replaced with
419 the corresponding promoters using 5' overhangs introduced by PCR primers. The
420 pBTK570 backbone was amplified and linearized into two fragments using the primer
421 pairs AC436/38 and AC435/39 for CP25; AC384/38 and 386/39 for CP6; AC388/38 and
422 387/39 for CP7; AC390/38 and 389/39 for CP32; AC392/38 and 391/39 for CP20; AC394/38
423 and 393/39 for J23100; AC396/38 and 395/39 for J23106 and AC398/38 and 397/39 for
424 J23116.

425 To generate the arabinose-responsive strains, we built the plasmids pAC51b,
426 pAC51c, pAC51g, pAC51i and pAC51j. Plasmid pAC51b was constructed by amplifying
427 the *araC* gene from pBAD33 using primers AC271 and AC272, and inserting it into the
428 pAC17v5b backbone, which was linearized into two fragments by PCR with primer pairs
429 AC273/49 and AC274/50. Plasmid pAC51c was assembled by cloning a chemically
430 synthesized pBAD25 promoter sequence, amplified with primers AC275 and AC276, into
431 the pAC17v5a backbone, also linearized into two fragments using primer pairs
432 AC019/059 and AC022/060. Plasmid pAC51g was generated by amplifying *araC* from
433 pAC51b using primers AC507 and AC09, and inserting it into the intermediate plasmid
434 pAC51e, which was linearized with primer pairs AC59/69 and AC504/60. Plasmid
435 pAC51e itself was built by cloning the *E2-crimson* gene, amplified from pBTK570 with
436 primers AC499 and AC501, into the pAC51c backbone, which was linearized with primer
437 pairs AC503/059 and AC504/060. Plasmid pAC51i was assembled by rejoining the
438 pAC51b backbone, amplified as three fragments with primer pairs AC516/010, AC18/050
439 and AC049/517. During amplification, the promoter CP25 was replaced by CP6 using the
440 5' overhang of primer AC517. Plasmid pAC51j was constructed by inserting the *gfp* gene,
441 amplified from pAC51c with primers AC518 and AC009, into the pAC51b backbone
442 linearized with primer pairs AC049/069 and AC274/050.

443 To generate the standardized suicide plasmids for homologous recombination in *S.*
444 *alvi*, we constructed plasmids pAC62, pAC98, pAC114 and pAC115. Plasmid pAC62 was
445 built by amplifying the R6K origin of replication from pKD3 using primers AC351 and
446 AC352 and inserting it into pBTK570, which was linearized with primers AC010 and
447 AC350. Plasmid pAC98 was assembled by amplifying the *kanR* cassette from pBTK519
448 with primers AC010 and AC447 and cloning it into pAC62 linearized with primers AC018
449 and AC448. Plasmid pAC114 was generated by amplifying the *ampR* cassette from
450 pAC08 using primers AC010 and AC541 and inserting it into pAC98 linearized with
451 primers AC018 and AC540. Plasmid pAC115 was constructed by cloning the *tetR* gene,

452 amplified from the genome of *S. alvi* using primers AC531 and AC532, into the pAC98
453 backbone linearized with primers AC533 and AC534, together with a short double-
454 stranded DNA fragment formed by annealing complementary oligonucleotides AC538 and
455 AC539.

456 Fragments were assembled using the NEBuilder HiFi DNA Assembly kit
457 according to the manufacturer guidelines. Sequences of cloning primers and synthesized
458 DNA can be found in **Supplementary Table 1** and **Supplementary Table 2**, respectively.
459 Full plasmid maps of suicide backbones and arabinose constructs are depicted in
460 **Supplementary Fig. 2a** and **Supplementary Fig. 3c**, respectively. The pBAD33 vector
461 was kindly provided by Prof. David Tirrell (California Institute of Technology, United
462 States)[51]. The pAC17v5a (Addgene plasmid No. 197413), pAC17v5b (No. 197414) and
463 pAC08 (No. #197402) plasmids were previously built by our group[30]. The pBTK570 (No.
464 110615) and pBTK519 (No. 110603) plasmids were a gift from Prof. Jeffrey Barrick[39]. The
465 pKD3 (No. 45604) plasmid was a gift from Barry L. Wanner[52].

466

467 **Engineering of *S. alvi* for arabinose biosensing.** To enable *S. alvi* to import arabinose, we
468 integrated the *araE* transporter into its genome *via* homologous recombination[43]. To
469 generate the *araE* insertion construct, we first retargeted the pAC98 backbone, carrying
470 the *kanR* cassette, to the *tetC* locus. Approximately 1 kb-homology arms flanking *tetC*
471 were amplified from the genome of *S. alvi* using primer pairs AC437/438 and AC439/440,
472 and inserted into the backbone, which was linearized into two fragments using the
473 primers AC010/216 and AC408/409 (**Supplementary Fig. 2**). These standardized primers
474 can be reused for retargeting any of the suicide plasmids, provided that the following
475 constant tail sequences are appended to the primers used to amplify the homology arms:
476 5'-cacttaacggctgacatggg-3' and 5'-catgaccaaaatcccttaacgtg-3' for one arm, and 5'-
477 cggatttacaattcgtcgtgc-3' and 5'-catctgaatcatgcgcggat-3' for the other.

478 Using the *tetC*-retargeted plasmid, we generated the final *araE* insertion fragment
479 by overlap PCR. The *araE* coding sequence was amplified from the genome of *E. coli*
480 using primers AC449/450, while the homology arms and *kanR* fragments were amplified
481 from the retargeted plasmid with primer pairs AC446/477 and AC445/462. PCR products
482 were combined at equimolar ratios (0.1 pmol each) in 20 μl of MiliQ water and assembled
483 using 25 μl of high-fidelity DNA polymerase (Phanta master mix, Vazyme). The first
484 overlap-extension stage was performed with the following conditions: 5 min at 95 °C,
485 followed by 15 cycles of 20 sec at 95 °C, 1 min at 58 °C and 2.5 min at 72 °C; and a final
486 extension for 5 min at 72 °C. The resulting assembly was resolved on an agarose gel, and
487 the band of the expected size was gel purified. A second amplification stage was then
488 performed by mixing 2 μL of the purified overlap product with 2 μl of each of the 10 μM
489 primers AC445 and AC446, 20 μl of MiliQ water and 25 μl of high-fidelity polymerase.
490 Amplification was carried out with the following conditions: 5 min at 95 °C, 30 cycles of
491 20 sec at 95 °C, 30 sec at 58 °C and 2.5 min at 72 °C; followed by a final extension for 5 min
492 at 72 °C.
493 The final overlap product was purified and 1 μg of linear DNA was electroporated
494 into *S. alvi*. Successful genomic integration of the *araE* gene was confirmed by Sanger
495 sequencing of the *tetC* locus. The resulting strain was then transformed sequentially by
496 electroporation with plasmid pAC51b followed by pAC51c, yielding the biosensor strain
497 *S. alvi* ac02.
498
499 **Flow cytometry.** Cell fluorescence was quantified using a NovoCyte flow cytometer
500 (Agilent) and the NovoExpress software (version 1.4.1). To assess arabinose response of
501 *S. alvi* ac02 and its derivative strains, as well as measuring gene expression levels of *S.*
502 *alvi* carrying the synthetic low-strength promoters, single colonies were streaked as
503 bacterial lawns on TSA plates supplemented with the appropriate antibiotics and
504 incubated for 3-4 days as described above. Cells from each strain were then scraped from

505 the agar surface, resuspended in liquid TSB to an optical density of 1.0 (OD_{600} = 1), and
506 used to inoculate five biological replicates by diluting 1:300 in fresh TSB supplemented
507 with varying arabinose concentrations when required. To assess the specificity of the
508 response to arabinose, TSB was supplemented with 0.7 mM of either xylose, ribose, or
509 arabinose. After 3 days of growth, cultures were diluted 1:10 in sterile PBS for flow
510 cytometry analysis.

511 Fluorescent cells were identified using a two-step gating strategy: first, bacterial
512 cells were selected on a FSC-H/SSC-H plot; single cells were then isolated on a FSC-
513 A/FSC-H plot. Fluorescence of singlets was subsequently recorded using the FITC-H
514 channel for GFP (ex. 488 nm – em. 530/30 nm) and the PE-Texas Red-H channel (ex. 561
515 nm – em. 615/20 nm) for E2-crimson. Mean fluorescence values were calculated from a
516 minimum of 10,000 bacterial events per sample. An example of the gating strategy is
517 provided in **Supplementary Fig. 9**.

518

519 **Determination of the honeybee gut volume.** To estimate honeybee gut volume, we
520 quantified water loss following desiccation of dissected guts from 20 bees co-colonized
521 with *S. alvi* ac02 and either *G. apicola* ESL309 or *G. apis* ESL169, collected across multiple
522 cages from the experiment described below. At day 7 post-colonization, 10 bees were
523 sampled from the treatment in which bees were fed sugar water (SW) supplemented with
524 210 μM arabinose, and 10 additional bees were sampled from the treatment in which
525 bees were fed SW and pollen, to assess whether pollen consumption influenced gut
526 volume.

527 Each dissected gut was transferred into a pre-weighted 1.5 ml Eppendorf tubes,
528 and tubes were weighed again to determine fresh gut mass. Tubes were then left open
529 and placed in an oven at 65 °C (fan 100%). After 22h, tubes were closed, cooled at room
530 temperature for ~30 min, reopened, and weighed to obtain the dry mass. Tubes were
531 returned to the oven for an additional 4 h and weighed once more to ensure that the dry

532 mass had stabilized. Gut volume in μl was estimated assuming a density of 1 mg μl^{-1} and
533 calculated as the mass difference between fresh and dry gut weigh. As no significant
534 difference in gut volume was observed between bees fed pollen and those not fed pollen,
535 we used the overall mean volume of 19.1 μl for subsequent calculation.
536
537 **GC-MS quantification of arabinose.** Arabinose levels in the gut were compared between
538 MD bees and those colonized with a synthetic community of 25 native bee gut bacterial
539 strains comprising the *Bartonella*, *Bifidobacterium*, *Bombilactobacillus*,
540 *Commensalibacter*, *Frischella*, *Gilliamella*, *Lactobacillus* and *Snodgrassella* genera. Bees
541 were given sugar water and sterilized pollen *ad libitum* for ten days. The experiment was
542 duplicated using bees from different hives with 4 bees sampled per replicate per
543 condition. Full hindguts were collected from anesthetized bees and homogenized with
544 glass beads in 500 µl of deionized water. An aliquot of 125 µl was then centrifuged for 20
545 min at 4 °C and 20,000 g and the supernatant was stored at -80 °C.
546 Gut homogenates and calibration curves of individual sugars were prepared
547 identically. A 5 µl mixture of D-norleucine and vanillic acid internal standards was spiked
548 into 20 µl of each sample immediately before extraction with 100 µl of cold
549 acetonitrile:methanol (1:1, v/v). Samples were stored at -20 °C for 2 h, then centrifuged at
550 18,000 g for 20 min at 4 °C. The supernatant was transferred to a new plate and dried in a
551 speed vacuum concentrator. Samples were derivatized with 50 µl of 20 mg ml^{-1}
552 methoxyamine hydrochloride in pyridine for 90 min at 34 °C, followed by 50 µl of N-
553 Methyl-N-(trimethylsilyl)trifluoroacetamide (MSTFA) for 120 min at 45 °C.
554 Samples were then randomized and 1 µl was injected *via* autosampler into an
555 Agilent 8890/5977B GC-MSD with a 2:1 split ratio and inlet temperature of 280 °C.
556 Chromatography was performed using a VF-5MS column (30 m × 0.25 mm × 0.25 µm)
557 with 1 ml min^{-1} helium flow rate. The oven was held for 2 min at 125 °C, increased at 3
558 °C/min to 150 °C, 5 °C/min to 225 °C, 15 °C/min to 300 °C, 25 °C/min to 310 °C and held for

559 3.3 min. The mass spectrometer was run in scan mode over a mass range of 50-550 Da at
560 a scan rate of 3.2 scans/s. Sugar peak areas were quantified using Agilent MassHunter
561 Quantitative Analysis software (version 10.0). Metabolite peak areas were normalized
562 across samples using the median internal standard areas, and a linear regression curve of
563 metabolite concentration *vs* peak area was calculated for each sugar.
564
565 **Plasmids maintenance measurement.** For the assessment of pAC51b and pAC51c
566 stability, single colonies of *S. alvi* ac02 were inoculated into liquid TSB and grown under
567 three conditions, each with 10 biological replicates: (*i*) 30 µg ml^{-1} spectinomycin, 30 µg ml^{-1}
568 ampicillin and 25 µg ml^{-1} kanamycin (+ ab); (*ii*) 25 µg ml^{-1} kanamycin only (- ab); or (*iii*) 25
569 µg ml^{-1} kanamycin and 0.07 mM arabinose (- ab + ara). After 3 days of incubation,
570 cultures were serially diluted and plated onto both selective and non-selective TSA.
571 Plasmid maintenance was quantified as the proportion of colonies that grew on selective
572 plates relative to the total number of colonies on non-selective plates, corresponding to
573 cells maintaining both plasmids.
574
575 **Honeybee rearing and gut colonization.** Microbiota-deprived (MD) *Apis mellifera carnica*
576 bees were obtained from outdoor colonies maintained at the University of Lausanne (VD,
577 Switzerland), following previously described procedures[12]. Briefly, mature pupae were
578 sampled from brood frames and transferred to sterilized plastic emergence boxes. Pupae
579 were incubated at 35 °C with 75 % humidity for 3 days. Emerging adults were supplied
580 with sterile 1:1 (w/v) sucrose solution.
581 To confirm the absence of microbial contaminants, hindguts of two newly
582 emerged bees per box were dissected and homogenized in 1 ml sterile PBS. Homogenates
583 were plated onto nutrient agar (NA), columbia blood agar (CBA), brain-heart infusion
584 agar (BHI), LB and MRSA plates and incubated under aerobic (NA, LB), microaerophilic

585 (CBA) and anaerobic (BHI, MRSA) conditions. Emergence boxes were excluded if any
586 microbial growth was detected on the corresponding plates.

587 For mono-colonization, MD bees were individually fed 5 µl of *S. alvi* ac02
588 resuspended at OD_{600} of 0.1 in 1:1 (v/v) PBS:sucrose solution. For co-colonization with the
589 native gut community, gut homogenate stocks were prepared by pooling equal volumes
590 of homogenized hindguts from five hive bees. The colonization inoculum was generated
591 by mixing *S. alvi* ac02 at OD_{600} of 0.1 with a 1:10 (v/v) dilution of the gut homogenate stock
592 in PBS:sucrose solution. For co-colonization with *G. apicola* ESL309 and *G. apis* ESL169,
593 bees were fed a mixture containing *S. alvi* ac02 and either of the *Gilliamella* species to a
594 final OD_{600} of 0.1 and 1, respectively, in PBS:sucrose solution. *Gilliamella* strains carried
595 the plasmid pAC09 (Addgene plasmid No. 197403)[30] encoding the E2-crimson fluorescent
596 protein to enable *in vivo* visualization.

597 Following colonization, bees were maintained in sterile cup cages at 32 ℃ and 75
598 % humidity. For fecal bacterial load assays, mono-colonized bees were supplied with
599 sugar water containing 85 μM arabinose, and either 30 µg ml^{-1} ampicillin plus 30 µg ml^{-1}
600 spectinomycin ('+ ab') or no antibiotic ('- ab', '- ab + gc'). To assess the *in vivo* biosensor
601 response to arabinose, mono-colonized bees received sugar water supplemented with 30
602 µg ml^{-1} of each ampicillin and spectinomycin, together with 0, 10, 100 or 1,000 μM
603 arabinose. Bees co-colonized with *S. alvi* ac02 and *Gilliamella* were given one of three
604 diets: (*i*) sugar water with 60 µg ml^{-1} ampicillin, (*ii*) sugar water with 60 µg ml^{-1} ampicillin
605 and 210 μM arabinose, or (*iii*) sugar water with 60 µg ml^{-1} ampicillin and pollen provided
606 *ad libitum*.

607 As pollen autofluorescence interferes with imaging, pollen was removed from
608 cages two days prior to gut dissection. All supplemented feeding solutions (*i.e.*
609 antibiotics and arabinose) were replaced with freshly prepared solutions every 3 days to
610 maintain consistent molecule concentrations.

611

612 **Bacterial load quantification *via* fecal sampling.** To quantify the fecal abundance of *S.*
613 *alvi* ac02, fecal material was collected from bees at 7 and 14-day post colonization with
614 the engineered cells. Bees housed in cup cages were stunned with CO_2 and subsequently
615 placed on ice to immobilize them. While anesthetized, gentle pressure was applied
616 manually along the abdomen from the anterior end toward the stinger to induce
617 defecation directly into the cap of sterile 1.5 ml Eppendorf tubes. Samples were
618 maintained on ice throughout the collection period.

619 Fecal matter that was sufficiently liquid was immediately serially diluted 1:10
620 (v/v) in sterile PBS. For more viscous samples, feces were first resuspended in 4 l of
621 sterile PBS before performing the 1:10 serial dilution. Diluted samples were plated on TSA
622 agar supplemented with 30 μg ml^{-1} spectinomycin, 30 μg ml^{-1} ampicillin and 25 μg ml^{-1}
623 kanamycin to selectively recover *S. alvi* ac02. Colony forming unit (CFUs) were counted
624 after 3-4 days of incubation.

625

626 **Gut microscopy analysis.** To prepare samples for microscopy, honeybee hindguts were
627 collected seven days after inoculation with engineered *S. alvi* and *Gilliamella* and
628 immediately immersed in 4 % paraformaldehyde in PBS. Tissues were fixed overnight at 4
629 °C with gentle rotation, followed by three 30-min washes at room temperature in PBS.
630 Samples were then permeabilized and stained overnight at 4 °C in the dark with 5 μg ml^{-1}
631 4,6-diamidino-2-phenylindole (DAPI) prepared in PBS containing 1% Triton X-100. After
632 staining, excess dye was removed by washing in PBS, and the ileum was dissected,
633 mounted in PBS and overlaid with a coverslip (number #1.5).

634 Image acquisition was performed using a Nikon AX R laser scanning confocal
635 microscope (Nikon, Japan) and the software Nikon NIS-Elements C (version 5.42.06).
636 Images were acquired with a 60X oil objective at 2048x2048 pixel format size (field of
637 view: 294.6278x294.6278 μm) and an averaging of 4 images. Pinhole size was set to 0.3
638 airy units, yielding an optical sectioning of 0.32 μm. Fluorescence acquisition was

performed sequentially in two passes to minimize crosstalk: E2-crimson (ex. 561 nm–em. 623-750 nm) and GFP (ex. 488 nm–em. 499-551 nm), followed by DAPI (ex. 405 nm–em. 420-551 nm).

For quantitative fluorescence analysis, all ileums were imaged using identical laser intensity and detector gain settings. For each gut, three regions were imaged: anterior, mid-ileum, and posterior. For each region, Z-stacks were also collected over a maximum depth of 40 µm with 1 μm step increment. Fluorescence quantification was automated using a custom Fiji macro developed for this study (see **Supplementary Text 1**). The macro was executed in Fiji (ImageJ2, version 2.16.0). Briefly, bacterial areas were segmented by applying a GFP fluorescence threshold identical across images. The resulting selected areas were copied to the corresponding DAPI images. For each region, mean fluorescence intensity per unit area was extracted for both GFP and DAPI channels. GFP intensities were normalized to DAPI intensities from the same segmented area to account for variation in cell density. When appropriate, normalized values from the three ileum regions were averaged to obtain a single fluorescence measurement per bee gut.

Acknowledgements

We acknowledge Lucy Genier for her support in the laboratory with molecular biology work. We thank Ly Pheak Chhun and Gonçalo Matos for helpful scientific discussions throughout the project. We also thank Georgia Petsiou for assistance with the bee experiments and Estelle Pignon for providing the *Gilliamella* strains bearing the pAC09 plasmid. We are grateful to Silvia Moriano Gutierrez for proofreading the manuscript, and to Méline Garcia for identifying the *Gilliamella* species of interest.

This work was supported by the University of Lausanne, the NCCR Microbiomes (National Centre of Competence in Research), funded by the Swiss National Science Foundation (grant no. 180575) to P.E and Y.S. The funders had no role in study design, data collection and analysis, decision.

666

667 ## Author contributions

668 A.C., P.E. and Y.S. conceived the study. A.C. designed the experiments and performed
669 molecular biology work, confocal microscopy, image analysis for fluorescence
670 quantification and bee experiments with support from F.Z. Suicide plasmids were
671 designed and built by A.C. and T.S. GC-MS arabinose measurements and related bee
672 experiments were carried out by A.Q. and T.H.G.N. Y.S. and P.E. supervised the project.
673 A.C. wrote the manuscript with input from co-authors.

674

675 ## Data availability

676 The plasmids developed in this study have been deposited in Addgene and are available
677 *via* the following accession numbers: pAC62 (#249659), pAC98 (#249660), pAC114
678 (#249661), pAC115 (#249662), pAC51b (#249663) and pAC51c (#249664). Confocal
679 microscopy images have been deposited in the BioImage Archive under the accession
680 number S-BIAD2461. Source data are provided with this manuscript.

681

682 ## Competing interests

683 The authors declare no competing interests.

684

685 ## References

686 1. Martinson, V. G. *et al.* A simple and distinctive microbiota associated with honey
687 bees and bumble bees. *Mol. Ecol.* **20**, 619–628 (2011).
688 2. Engel, P., Martinson, V. G. & Moran, N. A. Functional diversity within the simple
689 gut microbiota of the honey bee. *Proc. Natl. Acad. Sci.* **109**, 11002–11007 (2012).
690 3. Kwong, W. K. & Moran, N. A. Gut microbial communities of social bees. *Nat. Rev.*
691 *Microbiol.* **14**, 374–384 (2016).
692 4. Tang, J. *et al.* Synergistic pectin deconstruction is a prerequisite for mutualistic

693 interactions between honeybee gut bacteria. *Nat. Commun.* **15**, (2024).
694 5. Zheng, H. *et al.* Division of labor in honey bee gut microbiota for plant
695 polysaccharide digestion. *Proc. Natl. Acad. Sci. U. S. A.* **116**, 25909–25916 (2019).
696 6. Steele, M. I., Motta, E. V. S., Gattu, T., Martinez, D. & Moran, N. A. The Gut
697 Microbiota Protects Bees from Invasion by a Bacterial Pathogen. *Microbiol. Spectr.*
698 **9**, (2021).
699 7. Horak, R. D., Leonard, S. P. & Moran, N. A. Symbionts shape host innate immunity
700 in honeybees: Symbionts shape honey bee immunity. *Proc. R. Soc. B Biol. Sci.* **287**,
701 (2020).
702 8. Sato, Y. *et al.* Insecticide resistance by a host-symbiont reciprocal detoxification.
703 *Nat. Commun.* **12**, 1–8 (2021).
704 9. Liberti, J. *et al.* The gut microbiota affects the social network of honeybees. *Nat.*
705 *Ecol. Evol.* **6**, 1471–1479 (2022).
706 10. Vernier, C. L. *et al.* Gut microbiota contribute to variations in honey bee foraging
707 intensity. *ISME J.* **18**, (2024).
708 11. Cabirol, A., Schafer, J., Neuschwander, N., Kesner, L. & Liberti, J. A defined
709 community of core gut microbiota members promotes cognitive performance in
710 honey bees. *BioRxiv* https://doi.org/10.1101/2023.01.03.522593 (2023).
711 12. Kešnerová, L. *et al.* Disentangling metabolic functions of bacteria in the honey bee
712 gut. *PLOS Biol.* **15**, 1–28 (2017).
713 13. Quinn, A. *et al.* Host-derived organic acids enable gut colonization of the honey bee
714 symbiont Snodgrassella alvi. *Nat. Microbiol.* **9**, 477–489 (2024).
715 14. Callegari, M. *et al.* Compartmentalization of bacterial and fungal microbiomes in
716 the gut of adult honeybees. *npj Biofilms Microbiomes* **7**, (2021).
717 15. Richardson, M. *et al.* SAMPL-seq reveals micron-scale spatial hubs in the human
718 gut microbiome. *Nat. Microbiol.* **10**, 527–540 (2025).
719 16. Albenberg, L. *et al.* Correlation between intraluminal oxygen gradient and radial

720 partitioning of intestinal microbiota. *Gastroenterology* **147**, 1055-1063.e8 (2014).
721 17. Stüwe, M. & Liebeke, M. From microbes to molecules: unveilinghost-microbe
722 interactions withspatial metabolomics. *Mol. Syst. Biol.* **21**, 947–951 (2025).
723 18. Zhou, G. *et al.* Honeybees fed D-galactose exhibit aging signs with changes in gut
724 microbiota and metabolism. *mSystems* **10**, (2025).
725 19. Tang, M. *et al.* Honeybee-Gilliamella synergy in carbohydrate metabolism
726 enhances host thermogenesis in cold acclimation. *npj Biofilms Microbiomes* **11**,
727 (2025).
728 20. Brochet, S. *et al.* Niche partitioning facilitates coexistence of closely related gut
729 bacteria. *Elife* **10**, 1–23 (2021).
730 21. Oertel, E., Fieger, E. A., Williams, V. R. & Andrews, E. A. Inversion of Cane Sugar in
731 the Honey Stomach of the Bee. *J. Econ. Entomol.* **44**, 487–492 (1951).
732 22. Nicolson, S. W. The importance of osmosis in nectar secretion and its consumption
733 by insects. *Am. Zool.* **38**, 418–425 (1998).
734 23. Min, X. *et al.* Spatially resolved metabolomics: From metabolite mapping to
735 function visualising. *Clin. Transl. Med.* **14**, (2024).
736 24. Geier, B. *et al.* Spatial metabolomics of in situ host–microbe interactions at the
737 micrometre scale. *Nat. Microbiol.* **5**, (2020).
738 25. Geier, B., Oetjen, J., Ruthensteiner, B., Polikarpov, M. & Gruber-vodicka, H. R.
739 Connecting structure and function from organisms to molecules in small-animal
740 symbioses through chemo-histo-tomography. *Pnas* **118**, 1–9 (2021).
741 26. Bourceau, P. *et al.* Visualization of metabolites and microbes at high spatial
742 resolution using MALDI mass spectrometry imaging and in situ fluorescence
743 labeling. *Nat. Protoc.* **18**, 3050–3079 (2023).
744 27. Lötstedt, B., Stražar, M., Xavier, R., Regev, A. & Vickovic, S. Spatial host–
745 microbiome sequencing reveals niches in the mouse gut. *Nat. Biotechnol.* **42**, 1394–
746 1403 (2024).

747 28. Carreno, D. *et al.* Imaging of live bacterial whole-cell biosensors illuminates spatial
748 sialic acid availability within the inflamed mammalian gut. 1–45 (2024).
749 29. Rutter, J. W. *et al.* Detecting changes in the Caenorhabditis elegans intestinal
750 environment using an engineered bacterial biosensor. *ACS Synth. Biol.* **8**, 2620–
751 2628 (2019).
752 30. Chhun, A. *et al.* An engineered bacterial symbiont allows noninvasive biosensing
753 of the honey bee gut environment. *PLoS Biol.* **22**, 1–23 (2024).
754 31. Martinson, V. G., Moy, J. & Moran, N. A. Establishment of characteristic gut
755 bacteria during development of the honeybee worker. *Appl. Environ. Microbiol.* **78**,
756 2830–2840 (2012).
757 32. Kwong, W. K., Engel, P., Koch, H. & Moran, N. A. Genomics and host specialization
758 of honey bee and bumble bee gut symbionts. *Proc. Natl. Acad. Sci. U. S. A.* **111**,
759 11509–11514 (2014).
760 33. Ricigliano, V. A. *et al.* The impact of pollen consumption on honey bee (Apis
761 mellifera) digestive physiology and carbohydrate metabolism. *Arch. Insect*
762 *Biochem. Physiol.* **96**, 1–14 (2017).
763 34. Nicolson, S. W. & Thornburg, R. W. *Nectar chemistry*. (Springer, 2007).
764 doi:10.1007/978-1-4020-5937-7.
765 35. Campos, M. G. R. *et al.* Pollen composition and standardisation of analytical
766 methods . *J. Apic. Res. Bee World* **47**, 156–163 (2008).
767 36. Kolodrubetz, D. & Schleif, R. L-Arabinose transport systems in Escherichia coli K-
768 12. *J. Bacteriol.* **148**, 472–479 (1981).
769 37. Wagner, S. *et al.* Consequences of membrane protein overexpression in Escherichia
770 coli. *Mol. Cell. Proteomics* **6**, 1527–1550 (2007).
771 38. Zweers, J. C., Wiegert, T. & Van Dijl, J. M. Stress-responsive systems set specific
772 limits to the overproduction of membrane proteins in Bacillus subtilis. *Appl.*
773 *Environ. Microbiol.* **75**, 7356–7364 (2009).

774 39. Leonard, S. P. *et al.* Genetic Engineering of Bee Gut Microbiome Bacteria with a
775 Toolkit for Modular Assembly of Broad-Host-Range Plasmids. *ACS Synth. Biol.* **7**,
776 1279–1290 (2018).
777 40. Jensen, P. R. & Hammer, K. The sequence of spacers between the consensus
778 sequences modulates the strength of prokaryotic promoters. *Appl. Environ.*
779 *Microbiol.* **64**, 82–87 (1998).
780 41. Davis, J. H., Rubin, A. J. & Sauer, R. T. Design , construction and characterization of
781 a set of insulated bacterial promoters. *Nucleic Acids Res.* **39**, 1131–1141 (2011).
782 42. Leonard, S. P. *et al.* Engineered symbionts activate honey bee immunity and limit
783 Pathogens. *Science (80-.).* **576**, 573–576 (2020).
784 43. Lariviere, P. J. *et al.* One-step genome engineering in bee gut bacterial symbionts.
785 *MBio* **15**, (2024).
786 44. Stewart, P. S. & Franklin, M. J. Physiological heterogeneity in biofilms. *Nat. Rev.*
787 *Microbiol.* **6**, 199–210 (2008).
788 45. Stewart, P. S. *et al.* Reaction-diffusion theory explains hypoxia and heterogeneous
789 growth within microbial biofilms associated with chronic infections. *npj Biofilms*
790 *Microbiomes* **2**, 1–8 (2016).
791 46. Tropini, C., Earle, K. A., Huang, K. C. & Sonnenburg, J. L. The Gut Microbiome□:
792 Connecting Spatial Organization to Function. *Cell Host Microbe* **21**, 433–442 (2017).
793 47. Zeng, X. *et al.* Gut bacterial nutrient preferences quantified in vivo. *Cell* **185**, 3441–
794 3456 (2022).
795 48. Barker, R. J. & Lehner, Y. Influence of Diet on Sugars Found by Thin-layer
796 Chromatography in Thoraces of Honey Bees, Apis mellifera L. *J. Exp. Zool.* **188**,
797 157–164 (1974).
798 49. de la Fuente, M., Peñas, P. F. & Sols, A. Mechanism of mannose toxicity. *Biochem.*
799 *Biophys. Res. Commun.* **140**, (1986).
800 50. Liolios, V., Tananaki, C. & Dimou, M. Exploring the sugar profile of unifloral bee

801 pollen using high performance liquid chromatography. **57**, 341–350 (2018).

802 51. Kozlowski, M. T., Silverman, B. R., Johnstone, C. P. & Tirrell, D. A. Genetically

803 Programmable Microbial Assembly. *ACS Synth. Biol.* **10**, 1351–1359 (2021).

804 52. Datsenko, K. A. & Wanner, B. L. One-step inactivation of chromosomal genes in

805 Escherichia coli K-12 using PCR products. *Proc. Natl. Acad. Sci. U. S. A.* **97**, 6640–

806 6645 (2000).

807